The RIC Arm—A Small Anthropomorphic Transhumeral Prosthesis

Tommaso Lenzi, *Member, IEEE*, James Lipsey, and Jonathon W. Sensinger, *Senior Member, IEEE*

***Abstract*—Recent advances in motor and gear designs have accelerated the development of multi-degree of freedom prosthetic limbs controlled by novel electromyographic signal processing techniques. Most of these new devices have focused on improved performance at the expense of other critical factors for clinical use, such as weight and bulk, which significantly affect cosmesis and comfort. This paper presents the mechatronic design of an anthropomorphic transhumeral prosthetic arm—the Rehabilitation Institute of Chicago (RIC) arm—that is small enough for a 25th percentile female and weighs only 1518 g. Specifically, we describe the design of the RIC arm, including the integration of custom external rotor motors, cycloid transmissions, nonbackdrivable clutches, and custom pattern recognition control. Mechanics and control performance of the RIC arm were evaluated within the laboratory, and clinical viability was preliminary evaluated during a take-home field trial by an individual with a transhumeral amputation.**

***Index Terms*—Cycloid transmission, exterior-rotor motor, humanoid robots, lightweight robotic arm, prosthetics.**

I. Introduction

REPLICATING the functions of the human arm in a myoelectric prosthesis is a challenging design problem [1] that has captured the passion of engineers since 1940s [2]. More recently, significant resources devoted to prosthetics and robotics research have led to improved devices that allow users to control multiple degrees of freedom (DOFs) more intuitively [3]. Technological advances, such as embedded controllers, lithium-ion batteries, and brushless motors have enabled higher performance hardware. The human–machine interface has evolved due to the use of more sophisticated electromyographic (EMG) processing algorithms, such as machine learning [4] and finite-state machine [5], and a novel surgical technique—targeted muscle reinnervation—that improves the selectivity of EMG drives [6]. However, despite these technological and scientific advances, it is estimated that only 50%–60% of persons with an upper limb amputation wear a prosthesis at all [7], [8], and of those, only 40%–60% wear a myoelectric device [9].

Development of myoelectric prostheses has mostly focused on increasing the number of DOFs while increasing joint speed and torque [10]. Most recently, the convergence of robotics research and upper limb prosthetics has resulted in multiarticulating hand designs [11] and advanced control strategies (e.g., [12]–[14]). However, these devices achieve improved dexterity at the cost of increased weight, size, and complexity, which reduces robustness. Similarly, recent designs of experimental prosthetic systems that include anthropomorphically sized wrists (e.g., [10], [15]) have sacrificed weight considerations to achieve higher torque and speed performance. However, several recent surveys [7], [16], [17] have suggested that, for end users, appropriate prosthesis size and weight is as important as torque and speed performance. Reduced prosthesis size allows for better cosmesis for a broader population of users, while low weight reduces discomfort when the prosthesis is worn for extended periods. Thus, there remains a need for a cosmetically appealing prosthetic arm that is compact and lightweight enough to be comfortable for everyday use, while providing sufficient functionality to allow users to perform the most important activities of daily living. To address this need, we developed a novel transhumeral myoelectric prosthesis—the Rehabilitation Institute of Chicago (RIC) arm—that balances the tradeoff between performance and complexity with the ultimate goal of improving clinical use.

Reducing the weight and size of a prosthesis is not a trivial endeavor. Prostheses must be sophisticated enough to imitate the movement of the human arm, but all necessary actuators, transmissions, and electronics must be housed within the device to achieve cosmesis. Given these design constraints and the limitations of available EMG-based controllers [3], replicating the full kinematics and kinetics of the human arm is not feasible. For the design of our arm, we first selected the number and location of active DOFs that would allow for maximum functionality during activities of daily living. Then, we maximized the torque and energy density of arm actuators by developing custom motors and transmission systems. Finally, we developed custom electronics to provide good cosmesis, while minimizing electric energy consumption.

The RIC arm has five active DOFs, including a 2-DOF actuated hand, a 2-DOF wrist, and a 1-DOF elbow. The entire arm is sized to fit a 25th percentile female [18] (see Fig. 1) and includes a self-contained battery and an embedded pattern recognition controller. This paper presents the mechatronic design of the RIC arm, including its custom brushless motors and transmission design (see Section II), the integration of the

Manuscript received January 25, 2016; revised May 17, 2016 and July 25, 2016; accepted July 25, 2016. Date of publication August 10, 2016; date of current version December 13, 2016. Recommended by Technical Editor K. Oldham. This work was supported in part by the U.S. Department of Defense under Grant W81XWH-10-2-0033 and Grant W81XWH-11-1-0720, and in part by the Canada Natural Sciences and Engineering Research Council under Grant RGPIN 2014-06464.

T. Lenzi and J. Lipsey are with the Rehabilitation Institute of Chicago, Chicago, IL 60611 USA (e-mail: lenzi@northwestern.edu, jim.lipsey@ricres.org).

J. W. Sensinger is with the Institute of Biomedical Engineering, University of New Brunswick, Fredericton, NB E3B 5A3, Canada (e-mail: sensinger@ieee.org).

Color versions of one or more of the figures in this paper are available online at http://ieeexplore.ieee.org.

Digital Object Identifier 10.1109/TMECH.2016.2596104

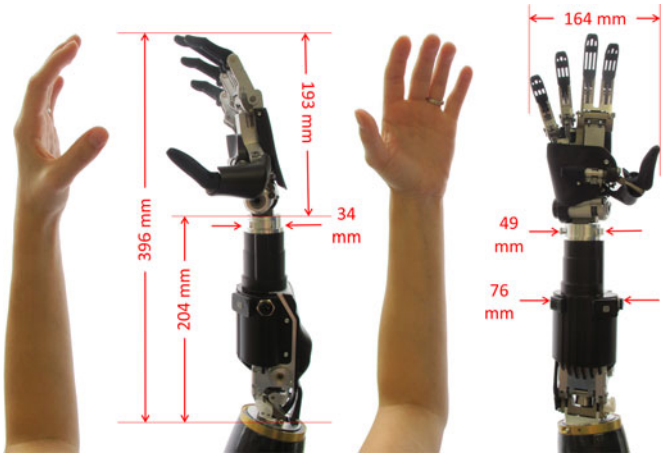

Fig. 1. RIC prosthetic arm compared with the 25th percentile female arm.

active DOFs (see Section III), and their performance characterization (see Section IV). Finally, we provide the results from a preliminary take-home trial of the arm (see Section V) by a transhumeral amputee.

II. Enabling Technologies

A. Exterior-Rotor Motor

Commercially available prostheses are powered exclusively by electric motors [11], due to their high power density. However, electric motors provide high power density only at high speeds, whereas human limbs operate at low speeds and high torques. Weaker motors necessitate bigger transmissions, which in turn substantially increase weight (the transmission weighs twice as much as the motor in a conventional prosthesis joint) and increase noise (since the fastest moving parts are moving faster). Thus, there is a need for motors that can provide high torque and slower speeds to reduce the size and weight of the transmission and to decrease the noise.

Conventional electric motors are typically compared based on rated power, but this metric is not selective enough for prosthesis applications. For a particular motion profile, the torque available to a motor is limited by the back-electromotive force (EMF) caused by its speed. Torque is further distributed between overcoming the inertia of the actuator and applied torque. These three factors (speed, torque, and inertia) are a function of the voltage across the windings and the current that can flow through them (limited either by the resistance of the windings, the rated current of the battery, or the thermal dissipation capacity of the motor). In a previous study, we demonstrated that these interacting factors can be taken into account by looking at the motor speed ratio [19]. Thus, comparing motors on the basis of speed ratios allows selection of the optimal motor topology for prosthetics or human–robotics applications.

Exterior-rotor motors produce substantially more torque for a given size than interior-rotor motors. This greater torque is in large part due to a larger air-gap diameter, which in turn is due to the fact that when balancing flux, the depth of the rare-earth magnet can be smaller than the length of the wire coil [20]. Interestingly, even though exterior-rotor motors have increased inertia (since the spinning part is on the outside, and inertia is proportional to the fourth order of diameter), the same or even higher speed ratios, compared to conventional motors, can be achieved by careful selection of rotor bell materials and geometry and making use of the substantially greater available motor torque.

Custom exterior-rotor motor with pole/tooth combination of 14/12 and a WYE termination were optimized for the RIC arm using SPEED design software [see Fig. 2(a)]. The stator teeth are wrapped with three-phase single span windings resulting in three sets of wires looped around the stator. The winding pattern is AacCBbaACcbB, where capital letters denote clockwise winding, lower-case letters denote counterclockwise winding, and A, B, and C denote the three phases. In addition, our custom motors use NdFeB N50 neodymium magnets, with M19 laminated teeth and a thin coating of paralyne to reduce the space lost to insulation around the teeth. Our custom motors achieve a net fill factor of 62%, which borders on the 70%–75% net fill factor obtained using rectangular wire [21]. Our motors have up to twice the speed ratio density of other motors typically used in prosthetic devices [20]. The increased torque reduces the motor speed during prosthesis operation, thus lowering the noise. In addition, it allows for a smaller transmission, thus reducing the weight and size of the prosthetic arm.

B. Cycloid Transmission

Prosthesis transmissions must be robust, lightweight, and, as they are typically paired with weak motors, have large gear ratios. In addition, they must be efficient—not only at high torques (where most manufacturers report efficiency) but also at low torques, since the majority of movements performed by users are low-torque movements. Harmonic drives and cycloid drives have the same typology [22] and achieve high gear ratios in a compact single stage with high efficiency compared to alternative transmissions, such as planetary gears [23]. Harmonic drives have been used for decades in the Boston Digital Arm (Liberating Technologies, Inc.) as well as in other research arms [24]–[26]. However, they are noisy, and, due to the requirement for elliptical ball bearings, difficult to scale down to small sizes while retaining high efficiency. Cycloid transmissions have recently been used in the Michelangelo hand (Ottobock USA) and offer a quiet alternative that achieves high efficiency even at low torques.

Based on our previous theoretical studies [27], we scaled the cycloid transmissions to a variety of sizes, as required by the different DOFs of the RIC arm. Although our initial designs used large gear ratios of 100:1 with free-rolling rollers [23], the cycloid drives implemented on the RIC arm have a 16:1 transmission ratio and fixed rollers directly placed in the grounded annulus. This deign change was motivated by the fact that the efficiency of cycloid drives is severely impaired for large gear ratios [22], and that fixed-rollers are more efficient than free rollers if the profile of the fixed-roller gear is optimized in light of the interaction between the fixed ring-gear and cycloid gear [28].

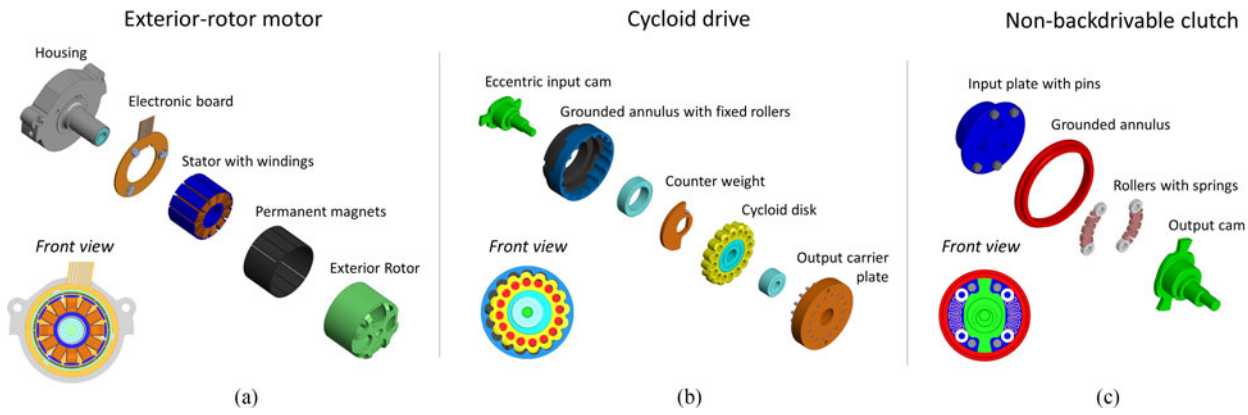

Fig. 2. Exploded and frontal views of the custom (a) exterior-rotor motor, (b) cycloid transmission, and (c) nonbackdrivable clutch as implemented on the wrist flexor joint.

Our final design of the cycloid drive for the wrist flexor [see Fig. 2(b)] comprises an eccentric input cam, a grounded annulus with fixed rollers (i.e., a fixed-roller gear), a cycloid disk (i.e., cycloid gear), an output carrier plate, and a counterweight, which is attached to the eccentric input shaft at 180° out of phase with the cycloid disk to cancel out oscillatory vibrations. The outer diameter of the cycloid transmission is 23 mm; the input eccentricity is 0.57 mm, the roller diameter is 1 mm, and the roller offset diameter is 20 mm. Our custom cycloid drive can withstand a continuous torque of 30 N·m and is equipped with mechanical fuses to prevent failure of the transmission in the event of higher torques generated outside of normal operating conditions. The custom cycloid drives allow the RIC arm to achieve high efficiency for a wide range of torque at a lower weight than traditional transmission systems.

C. Nonbackdrivable Joints

Nonbackdrivable transmission systems allow a joint to hold a position independently of the torque applied to the joint output, without providing any motor torque. In the RIC arm, we use nonbackdrivable clutches [29] in series with high-efficiency transmission components, such as planetary gears and cycloid drives at the elbow and wrist joints. The nonbackdrivable clutches at each joint in the RIC arm follow similar working principles [see Fig. 2(c)]. The nonbackdrivable clutch comprises an input plate with two couples of symmetric pins, a grounded annulus, an output cam, and four rollers connected to two springs that ensure the rollers are in contact with the grounded annulus when the system is at rest. When the motor is actively driving joint movement, two pins on the input plate push the rollers out of contact with the grounded annulus and engage the output cam, allowing the motor to drive the movement of the active DOF. In contrast, if movement is attempted from the output side of the nonbackdrivable clutch (i.e., the output cam), the jam angle between the grounded annulus, rollers, and output cam prevents movement [see front view in Fig. 2(c)]. Use of nonbackdrivable clutches saves a significant amount of electrical energy, allowing for a smaller, lighter battery, and, therefore, lowering the weight and size of the prosthetic arm.

III. Mechatronics Design

Selecting the appropriate number and location of the active DOFs in the design of a prosthetic arm is critical to find the optimal balance between dexterity and weight, and, ultimately, to optimize clinical benefit. Although robotics and mechatronics research has mostly focused on developing multiarticulating hand designs [11] and related controls [12]–[14] that attempt to imitate human hand kinematics, a recent clinical study [30] showed that a 22-DOF hand with a 1-DOF wrist is functionally equivalent to a 1-DOF hand and a 2-DOF wrist when performing activities of daily living, as measured by the Southampton Hand Assessment Protocol [31]. Based on these findings, we decided to develop a 2-DOF wrist and a 2-DOF hand, which would minimize prosthesis weight, size, and complexity, while providing sufficient functionality for the most common activities of daily living.

Another fundamental issue in the kinematic design of arm prosthesis is the relative orientation of the active DOFs with respect to the arm linkages. This defines the orientation and range of motion of the arm end point (i.e., the prosthetic hand) in space, thus affecting arm functionality. In contrast to conventional prosthetic elbows, the RIC arm has a 1-DOF elbow that captures the natural carrying angle of intact human elbows [32] (i.e., about 12° when the elbow is fully extended), causing the hand to be more lateral than the elbow when the arm is fully extended. This small but significant design innovation allows the prosthetic hand to reach the midline of the body when the elbow is flexed, without the need for medial/lateral humeral rotation (see Fig. 3). Merely imitating the physiological carry angle of the elbow improved prosthesis functionality without additional complexity or weight.

As for the elbow joint, the wrist flexor joint of the RIC arm is canted off-axis. However, in contrast to the elbow, where the physiological carrying angle was implemented, the canted angle at the wrist flexor was made to mimic the angle of a dart-thrower's hand, which couples wrist flexion with ulnar deviation. The prosthetic hand has 5° radial deviation offset and is rotated by 19° about the wrist rotator axis. Together with wrist pronation/supination, this modification allows the wrist

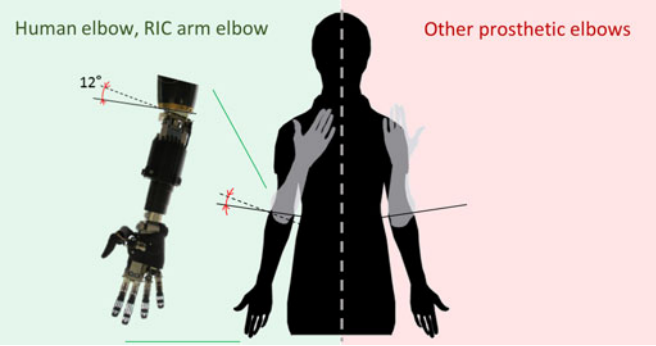

Fig. 3. Effect of the elbow carrying angle on the position of the hand in extended (black) and flexed (gray) positions. On the left, the human and RIC arm and on the right, other commercially available elbow prostheses.

to encompasses the path of the majority of activities of daily living [33]; thus, enabling the RIC arm to support a full range of functional activities without requiring a third DOF at the wrist, which, in turn, would have increased the weight and control complexity of the prosthesis. The Gen-3 DEKA arm also combines wrist flexion with radial/ulnar deviation [10].

A. Elbow Module

A partially sectioned view of the elbow module is shown in Fig. 4(a). The elbow uses a custom exterior-rotor motor, as described in Section II-A. The motor output shaft is connected to a low-profile single-stage planetary gear transmission with a transmission ratio of 4:1 that was customized from a stock gear (MicroMo, Clearwater, FL, USA). A nonbackdrivable clutch (see Section II-C) connects the planetary gear to a differential roller screw [34]. Roller screws combine the high efficiency of ball screws (our roller screw has ∼86% efficiency) with the ruggedness of lead screws and have recently been used in a prosthetic ankle [35]. Threaded planetary rollers take the place of screw threads, allowing rolling motion rather than sliding motion; thus, increasing efficiency, while withstanding the potentially high forces experienced by a prosthetic arm. Importantly, the nut of the differential roller screw pivots about a hinge joint, so the roller screw experiences axial loads but not bending moments. This hinge joint is enclosed in bushing made of a nonlinear compliant material (polyurethane), which allows the prosthetic elbow joint to mimic the natural arm-swinging movement of able-bodied persons during walking. Additionally, the nonlinearity of the compliance prevents the elbow joint from deforming too far when user needs to push on it. Finally, the differential roller–screw drives a four-bar mechanism that converts the linear motion of the screw to a revolute motion of the elbow joint, while providing a variable moment arm. The four-bar mechanism was optimized in SimMechanics (The Mathworks, Inc.) to obtain a nonlinear gear ratio that provides maximum torque over the range of movement most affected by gravity.

B. Wrist Rotator and Wrist Flexor Modules

The wrist rotator and flexor joints share the same actuator design [see Fig. 4(b)], which comprises a custom exterior-rotor motor, a single-stage planetary gear, a nonbackdrivable clutch [29], and a cycloid transmission. The wrist exterior-rotor motor has similar design to the elbow motor (see Section II-A). Table I lists design specifications for our final wrist motor (used in both the wrist flexor and rotator) and for the Maxon EC20 flat 5W, and the MicroMo 2036. These two commercially available motors are of similar size to the RIC motor, although the MicroMo 2036 is almost twice as long. The RIC motor had considerably larger stall torque (allowing for a lower gear transmission), motor constant (a winding-independent indication of torque), and speed ratio (allowing for more rapid, ballistic motions) and a lower peak speed than the other motors. Essentially, the RIC motor has an inherent "gear ratio" because of the increased number of pole pairs, which allows the use of a smaller gear transmission without negatively affecting performance on the output joint.

The RIC custom wrist motor was connected to a single-stage planetary gear transmission, modified from a stock MicroMo gear, which comprises a grounded annulus, a sun gear (input) connected to the motor output, planetary gears, and a carrier plate (output). The planetary gear transmission is coupled to a nonbackdrivable clutch (see Section II-C). In turn, the nonbackdrivable clutch is connected to a cycloid transmission, described in detail in Section II-B and shown in Fig. 2(c). The wrist cycloid drives were optimized based on our previous studies [23], [27] to provide minimum radial loading while maintaining a low-profile design without undercutting the gear-tooth profile. In its final configuration, the wrist flexor has dimensions of 35 mm × 45 mm × 58 mm, a mass of 142 g, and a no-load speed of 85 r/min. It can produce a stall torque of 2.5 N · m when powered at 14.8 V and drawing a current of 3.1 A. The wrist uses the latest version of the universal quick disconnect [36], developed by Motion Control, Inc., which enables the device to generate large wrist-rotator torques without unscrewing and provides uninterrupted bus communication even when the wrist is manually rotated.

C. Hand Module

The hand module (see Fig. 5) has been designed to achieve a wrap-around grasp, i.e., the object is held against the palm by the fingers wrapped around it, with the thumb opposing the index finger. A wrap-around grasp was a specific design requirement based on our polling of clinicians, which indicated that end users prefer a stable base rather than having the thumb and fingers move simultaneously. However, if the thumb is fixed to provide a stable base, and the hand is small, such as that of a 25th percentile female, grasping the majority of everyday objects (e.g., those requiring an 80-mm opening width [37]) requires a wrap-around grasp (see Figs. 5 and 6.).

The hand module (see Fig. 5) comprises a frame, to which fingers, thumb, motors, and related transmission elements are connected. The fingers are based on a four-bar linkage design that provides coupled flexion of the metacarpophalangeal (MCP) and proximal interphalangeal (PIP) joints (see Fig. 7) to allow a wrap-around grasp. In addition, mechanical compliance was added by embedding elastic elements (tension springs and custom tension elastic elements for the last two and first two fingers,

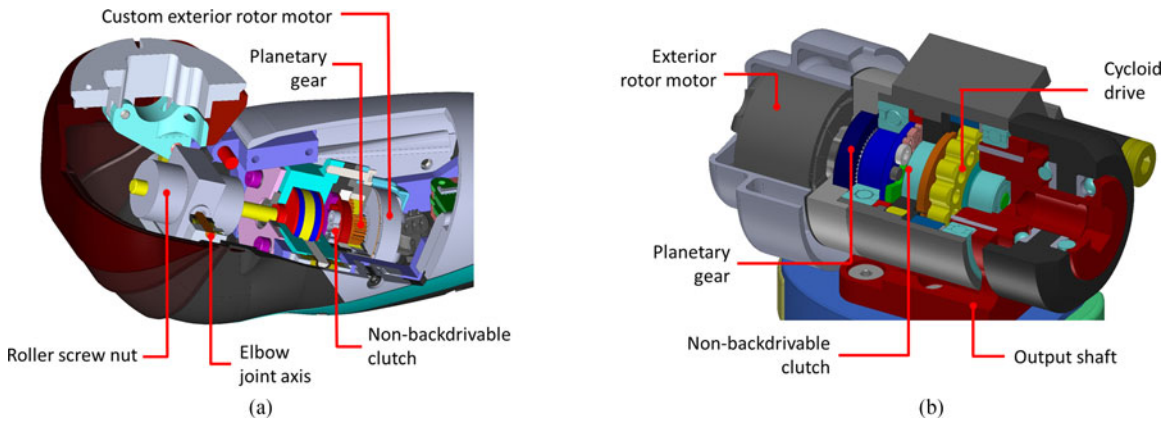

Fig. 4. (a) Partially sectioned view of the elbow module including a custom exterior-rotor motor, a planetary gear, a custom nonbackdrivable clutch, and a roller–screw acting as a slider in a four-bar linkage configuration. (b) Partially sectioned view of the RIC arm wrist, including a custom exterior rotor motor; a planetary gear transmission; a custom nonbackdrivable clutch; and a custom cycloid transmission.

TABLE I
WRIST MOTOR PARAMETERS

	RIC motor	Maxon EC20 flat (5W)	MicroMo 2036
Supply voltage (V)	14.8	14.8	14.8
No-load speed (r/min)	5000	11 569	21 706
Stall torque (mN · m)	89.7	23.31	27.13
Stall current (A)	4.5	1.99	4.31
Winding resistance (Ω)	3.3	7.45	3.4
Torque constant K_t (mN · m)	20	11.8	6
Motor constant $(^{\mathrm{mN}\cdot\mathrm{m}}/_{\sqrt{\mathrm{W}}})$	11	4.32	3.4
Speed Ratio (Hz)	237	36	62
Diameter (mm)	20	21.2	20
Height (mm)	20	14	36
Mass (g)	26	22	50

respectively) to one of the four-bar linkages that define finger kinematics (see Figs. 5 and 7).

All fingers have similar four-bar linkage design, although the elastic elements are arranged to act on the PIP joint in the first two digits [see Fig. 7(a) and (b)], and on the MCP joint in the lateral two digits [see Fig. 7(c) and (d)]. The compliance of the PIP joint in the first two fingers is restricted to 5° by limiting the extension of the custom elastic element located on the connecting link of the four-bar linkage [see Fig. 7(a)]. In contrast, in the last two digits, the helical tension spring that connects the proximal link of the finger to the actuator (see Fig. 5) provide torque on the MCP joint until it reaches its mechanical end stop.

The four fingers (eight joints) are driven by a single actuator, based on the clinical observation that wrist function is more important than individual finger function [30]. All fingers are actuated with a commercial brushless motor (EC10, Maxon Motors), with an integrated planetary (4:1) gear head connected through a spur gear to a satellite roller screw (Rollvis, Switzerland), which is in turn connected to the four-bar finger linkage. A nonbackdrivable clutch between the spur gear and the satellite roller–screw maintains grasp force without continuously consuming battery power. Essentially, this finger design is an underactuated mechanism with compliance and saturations optimized to ensure a biomimetic stable wrap-around grasp.

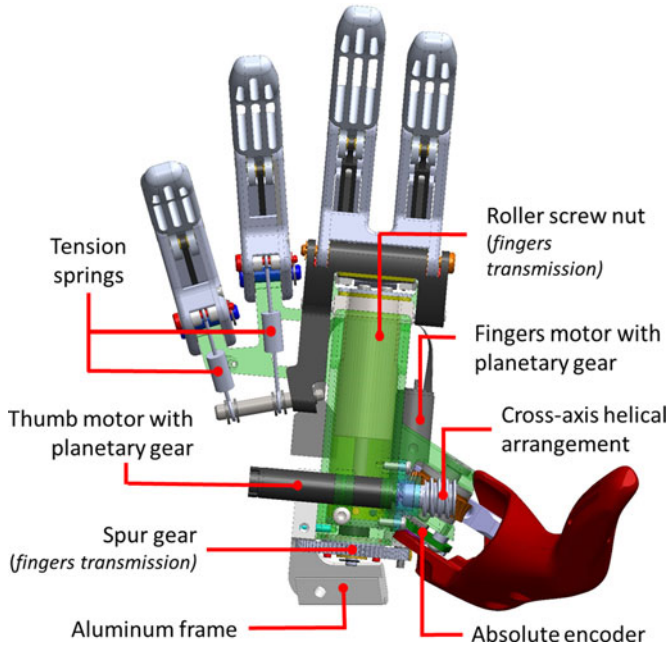

Fig. 5. Details of the RIC hand design, showing finger actuation (based on an off-the-shelf motor, primary spur gear, and secondary roller screw transmission with slider-crank configuration including linear springs for the third and fourth fingers) and thumb actuation (based on an off-the-shelf motor with integrated planetary transmission, and a secondary nonbackdrivable stage based on custom cross-axis helical arrangement).

The thumb oblique axis (see Fig. 5) is independently powered by a brushless motor (EC8, Maxon Motors) with an integrated 16:1 planetary gear (Maxon Motors), connected to a custom crossed-axis helical gear set with a 62° compound angle between axes. This cross-axis helical arrangement was designed to allow placement of the actuator independently of the axis of thumb rotation; thus, allowing the simultaneous alignment of the actuator in an inconspicuous arrangement while achieving the desired oblique axis of rotation of the thumb. The cross-axis helical arrangement is nonbackdrivable, thus obviating the need for a nonbackdrivable clutch. The final tilt angle of the thumb

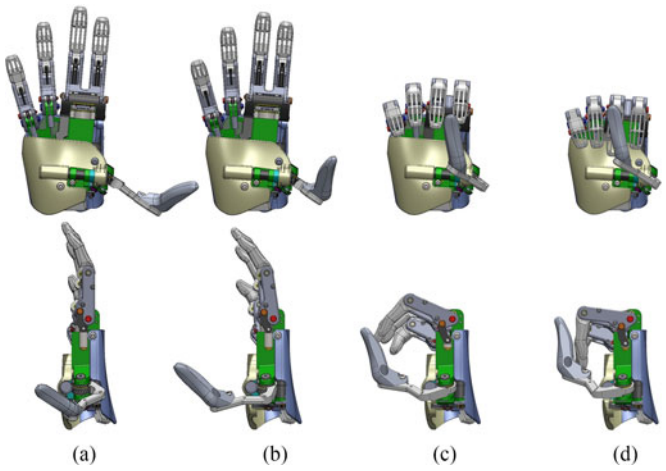

Fig. 6. Front and side views of the grasp patterns achieved using a single motor to drive the fingers, and a single motor to drive the thumb at an oblique axis. (a) Palm flat. (b) Open grasp. (c) Chuck grasp. (d) Cylindrical grasp.

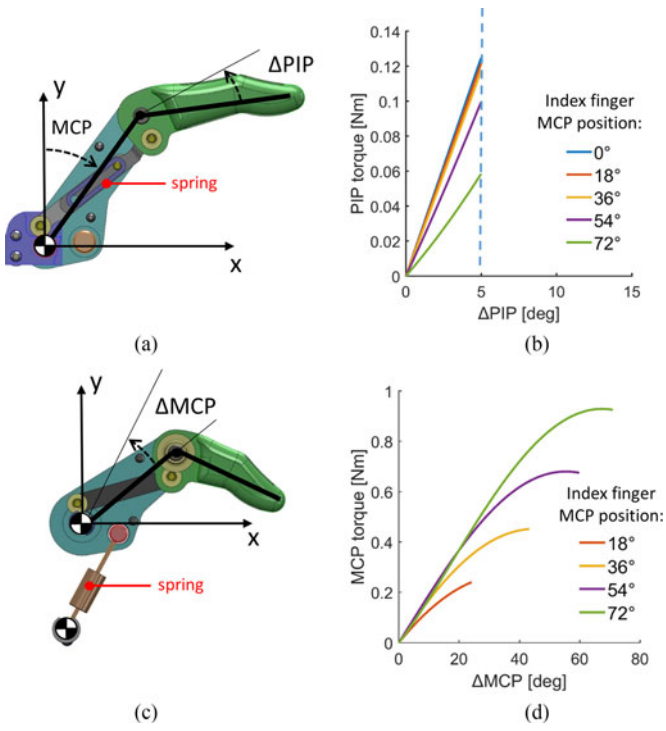

Fig. 7. Four-bar linkage, design and resulting elastic joint torque of the index/middle fingers [panels (a) and (b)] and annular/pinkie fingers (panels (c) and (d). Resulting joint torque/displacement curves for different actuator positions are shown at right; different colors represent different hand closing positions as indicated by the MCP and PIP resting positions shown by the legends in panels (b) and (d).

axis (i.e., thumb abduction), defined by the axis of this helical gear, was chosen after evaluating numerous prototype iterations with clinicians to ensure the tilt angle allowed for a variety of grasps. The hand is capable of achieving four grasp patterns, as shown in Fig. 6: palm flat (useful for holding trays, and pushing off a surface), hand-open (a natural looking hand-open posture),

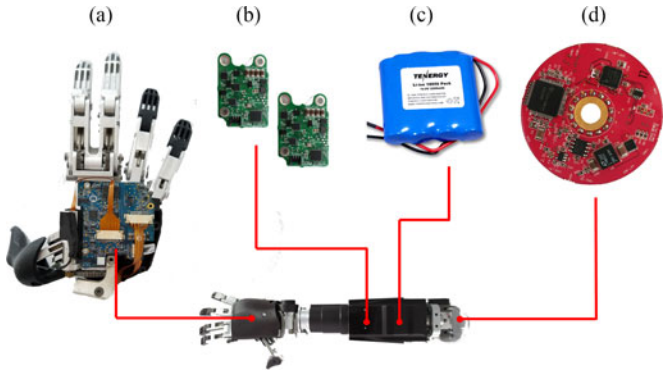

Fig. 8. Custom electronic boards and battery location within the RIC arm: (a) Hand electronic board comprising the CCU, and three motor controller logic boards for the fingers flexor, thumb, and wrist flexor; (b) motor servo controller electronics comprising motor controller logics and H-bridge—one boar each for the wrist rotator and elbow flexor; (c) Li-ion battery; and (d) front-end electronics.

chuck-grip (the most commonly used prosthetic grip posture in commercially available prostheses), and cylindrical-grip.

Both the RIC hand and the Michelangelo hand [11] have two active DOFs, although differences in numbers of joints and linkage kinematics result in distinct hand functionalities. Specifically, the RIC hand has articulated finger kinematics with intrinsic compliance and coupled MCP and PIP joint motion (see Fig. 7). In contrast, the Michelangelo fingers consist of a single stiff finger segment actuated at the MCP-joint with coupled flexion and abduction movements [11]. Moreover, the thumb of the RIC hand has a fixed abduction joint and actuated flexion joint; thus, the RIC hand can perform all available grasp patterns independently of finger movement. The thumb of the Michelangelo hand is prepositioned by a small motor into a specific grasp configuration prior to performing a grasp, which is then powered by the same motor that allows for finger flexion. Consequently, the Michelangelo hand can perform lateral pinch but not power grasp (cylindrical grip), whereas the RIC hand cannot perform lateral pinch but can perform power grip.

IV. System Architecture and Control

A. Electrical System

An overview of the RIC arm system architecture is shown in Fig. 9. The prosthesis uses a lithium-ion battery pack, which is housed in the prosthesis forearm, has 14.8-V nominal voltage, and is rated at 2200 mAh (Tenergy Li-Ion 18650). The embedded system comprises a front-end module, a user interface module, a central computing unit (CCU), and five motor servodrive modules. Each embedded module is configured to receive power from the main battery and is equipped with its own regulator (either 5 or 3.3 V) to properly power the logic unit and the connected devices and sensors. The CCU and three motor servodrive modules controlling the fingers, thumb, and wrist flexor joints are housed in the back of the hand, whereas the two motor servodrive modules controlling the wrist rotator and elbow flexor joints are located in the prosthesis forearm, together with the front-end module and the user interface mod-

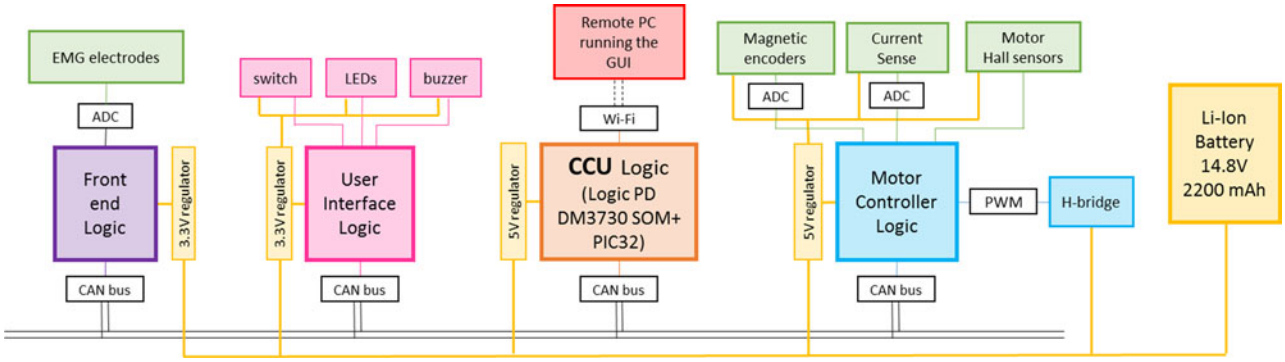

Fig. 9. Overview of the modular RIC arm system architecture, comprising a front end to record and preprocess electromyography signals, a basic user interface with a mechanical switch, buzzer and status LEDs, a main controller implementing pattern recognition control strategies while communicating with a remote PC through Wi-Fi, and dedicated motor control units for each active DOF with independent sensor acquisition and processing. Each of these system modules has a dedicated CAN-bus controller for fast and reliable communications, and a separate regulator to power the processing unit and the connected devices/sensors.

ule. A controller area network (CAN bus) interface allows the embedded modules to communicate, substantially reducing the number of wires, which both reduces the complexity and increases reliability and modularity of the RIC arm. Fig. 8 shows the final format of the RIC arm custom electronics.

The front-end module interfaces with the passive EMG electrodes, which that are placed in the socket so as to make direct skin contact with the user's residual arm. Up to eight bipolar electrode pairs can be connected to the front-end module, which acquires analog EMG signals at 1 KHz, applies a bandpass filter with a range of 85–350 Hz, amplifies the digitized and filtered signals with a fixed gain of 2, and transmits them on the CAN bus. The 85—350-Hz range of the bandpass filter allows the controller to avoid the noise due to the power line (i.e., 50–60 Hz), without a significant loss of information content in the acquired EMG signals [38].

The CCU runs the high-level control loop, which defines the speed of each DOF in real-time based on user movement intention, as determined from EMG signals. The CCU is housed within the prosthetic hand and comprises a system on module (DM3730, Logic PD, Minneapolis, MN, USA)—running a custom operating system based on Linux YOCTO—a PIC32, and CAN bus controller. The outputs to the main controller are transmitted using the CAN bus to motor servodrives of each active DOF. In addition, the CCU communicates through Wi-Fi with a remote computer that runs the graphical user interface (GUI). The GUI allows prosthetists or therapists to view the user's EMG signals online and tune prosthesis control parameters accordingly. The user can also interface with the arm CCU though the user interface module, which comprises a logic unit with CAN controller, a mechanical switch, multicolor LEDs, and a buzzer. The user interface module is used to turn the arm on or off and to start the calibration procedure that is required for pattern recognition control. The motor servodrives are responsible for low-level motor control, which is obtained through pulse-width modulation (PWM) signals that control the brushless motor MOSFET bridges. In addition, the servodrive modules acquire information from the active DOF sensors, which include absolute magnetic encoders on the elbow and thumb

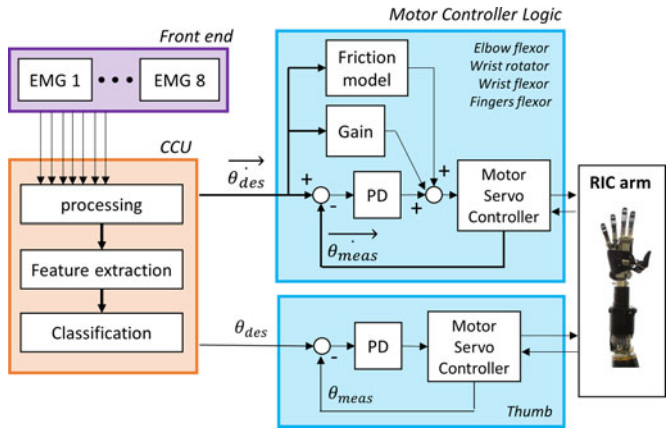

Fig. 10. Block diagram representation of the RIC arm controller. The pattern recognition controller receives the raw EMG signals from the front end, and outputs the desired velocity and position commands to the motor controllers through CAN-bus. The motor controller logic of all joints except the thumb implements a velocity control algorithm with a feedforward and a feedback node. The thumb position is controlled through a proportional-derivative feedback loop to implement the desired grasp patterns, as selected by the classifier.

joints, Hall-sensors on all motors, and current sensors. Again, acquired data are transmitted on the CAN bus. The motor servodrives are a customized version of motor controllers that were licensed from the Applied Physics Lab of John Hopkins University. The internal amplifiers provide high current (3.5 A in continuous) in a smaller size than commercially available alternatives.

B. Control system

A block diagram representation of the RIC arm controller is shown in Fig. 10. The RIC arm uses an advanced EMG processing technique, based on machine learning, which is commonly referred to as pattern recognition control [4], which runs on the RIC arm CCU. When pattern recognition control is active, appropriate features are extracted from raw EMG signals and correlated to the user's intended movements using a classifier

[39], which then defines the desired prosthesis joint velocities and grasp pattern. Specifically, the CCU receives raw EMG signals from the front-end module, processes them to obtain their mean absolute values, and extracts eight features (four time-domain and four autoregressive), using a linear discriminant classifier with a frame length of 250 ms and an overlap of 25 ms, as described in [40]. The classifier can discriminate up to 11 classes: no motion, elbow flexion, elbow extension, wrist flexion, wrist extension, wrist supination, wrist pronation, hand open, chuck grip, cylindrical grip, and fine-pinch grip. Movement classes can be selectively activated or deactivated by the therapist, based on the specific needs of each user. Finding the best correlation between EMG features and active DOF movement classes requires supervised training of the classifier, which is performed offline, starting from EMG data acquired during calibration sessions using prosthesis-guided training [41]. Calibration sessions, which are performed routinely by patients, are initiated through the user-interface module. The prosthesis then performs a series of movements in which all active DOF movement classes are performed sequentially. While the prosthesis moves, users attempt to perform the same movement with their missing limb, activating residual muscles, and generating corresponding EMG signals [41]. Calibration data are then processed offline to obtain a correlation matrix for online prosthesis control. Pattern recognition [4] and prosthesis-guided training allow multiple DOFs to be quickly and reliably controlled by persons with transhumeral amputations [40].

For each active DOF, the low-level control loop is implemented in the motor controller logic module, and consists of a hybrid velocity control loop with feedforward and a feedback commands. Specifically, the feedforward node outputs a desired PWM value that results from the sum of two terms. The first is the set point of the desired joint speed as defined by the EMG activations. The second compensates for friction in the actuation system, as it changes with joint speed. For each joint, feedforward friction compensation was based on the friction model described in [42], and tuned experimentally (e.g., as described in [43]). The most important impact of friction compensation on velocity controller performance is to allow the prosthesis joints to move smoothly at low desired speeds, by compensating for the presence of Coulomb friction in the transmission system. On the other hand, compensation for viscosity has a limited impact on joint performance, as the correlation between EMG activation and joint speeds is already defined by a tunable gain, which is set by the therapist/prosthetist when the user is fit with the RIC arm.

The feedback loop consists of a simple proportional-derivative compensator driven by the speed error, which is computed as the difference between the desired joint speed and the actual speed, estimated directly through the motor Hall-effect sensors. The feedback compensator enhances the dynamic response of the low-level control to speed commands and allows smooth velocity profiles over a wide range of speed commands, despite the limited accuracy of the Hall-sensor speed estimate. Unlike all other active DOFs, thumb joint velocity is not under the user's direct control. Rather than directly responding to EMG commands, the position of the thumb is determined based on the grasp pattern selected by the pattern recognition controller. As such, thumb position relies on a closed-loop position control, implemented in the thumb motor controller module, to achieve the desired hand grasp.

The low-level velocity controller was designed and tuned based on the specific requirements for high-level EMG control of motorized upper limb prostheses. Specifically, by omitting the integral term in the inner feedback loop, the implemented velocity controller does not compensate for possible external loads applied to the arm. As a consequence, if an external resistive load is applied to the prosthesis while the velocity command is kept constant, the prosthetic joints subjected to the load will slow down. In addition, the proportional velocity controller gives users a basic way to regulate the maximum effort applied by the prosthesis joints on the environment. In fact, when the joint speed approaches zero (i.e., steady-state interaction with the environment), the velocity command approximates a force control, because of the linear relationship between applied motor voltage (proportional to PWM input) and motor current (proportional to motor torque). As a consequence, a low-velocity set point will always result in low joint torque at the steady state. However, the lack of force and tactile feedback may limit the ability of users to interact with the environment and to regulate the grasping force, as demonstrated in previous studies [12], [13].

V. Performance Characterization

Performance characterization experiments were performed to assess whether the custom motor, transmission, and power electronics allowed the RIC arm to achieve adequate performance in terms of speed range, linearity, dynamic response, pinch force, and operating autonomy on a single battery charge. The velocity set point was commanded with an external computer using the CAN-bus interface rather than using the high-level controller based on the EMG signals—i.e., we bypassed the front-end module and the CCU by sending velocity commands directly to the motor controller logics. Sampling frequency was set at 200 Hz, and the remote computer recorded the data.

To assess maximum joint speeds, and to quantify the linearity of the speed controllers at the steady-state, the full range of motion for each active DOF, except the position-controlled thumb, was tested back and forth at four different input speeds. Speeds were equally spaced within the input speed range of each joint. The maximum joint speed for each active DOF is reported in Table III, together with comparative data from other commercially available prosthetic components. The elbow joint achieved the slowest maximum speed, 80 °/s; the wrist rotator was the fastest joint, achieving a maximum constant speed of about 500 °/s, followed by the wrist flexor with 450 °/s. The finger MCP joints achieved a maximum speed of about 180 °/s, allowing the prosthetic hand to fully close in only 0.4 s. For all active DOFs, measured joint speed scaled linearly with desired speed. Linear fitting between desired and measured speed revealed root-mean-square errors of 1.71, 9.65, 9.91, 1.26 °/s (2.15%, 1.93%, 2.18%, 0.70%) for elbow, wrist rotator, wrist flexor, and finger MCP, respectively, with a minimum R-square among all active DOFs of 99.7. Cumulatively, the results of this

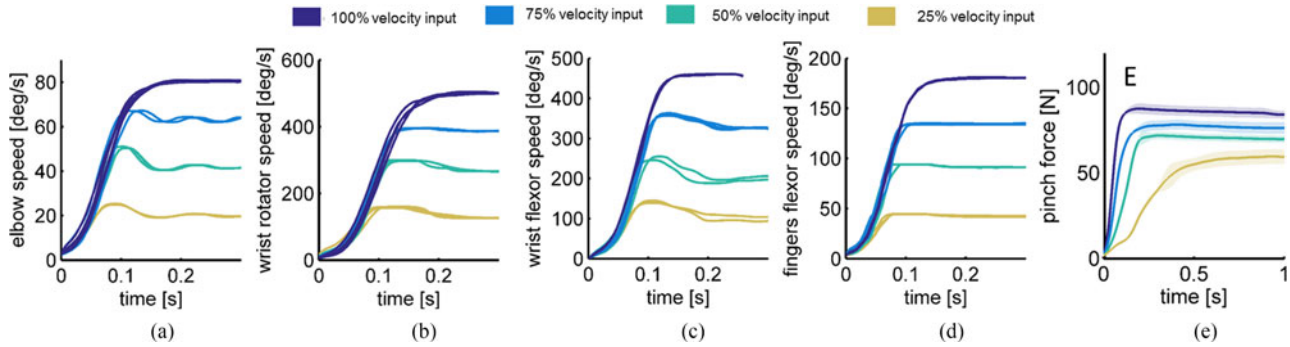

Fig. 11. Dynamic response to different velocity step inputs for unconstrained movements at the (a) elbow flexor, (b) wrist rotator, (c) wrist flexor, and (d) fingers flexor. (e) Pinch force response for four different hand velocity set point. Different colors show different speed inputs as shown in the legend above the Panels.

TABLE II
RISE TIME AND OVERSHOOT OF THE VELOCITY STEP RESPONSE

	Rise Time (ms)				Overshoot (°/s)			
Elbow Flexor	97	71	64	53	1	7.2	9.8	4.9
Wrist Rotator	104	79	65	64	0	8	24	20
Wrist Flexor	78	61	52	53	0	25	40	35
Fingers Flexor	81	59	52	55	0	5	3	2

TABLE III
PERFORMANCE METRICS

Hand	RIC	Otto Bock Michelangelo
Close time (s)	0.4	0.4
Pinch force (N)	84	70
Mass (g)	383	420
Wrist Rotator	RIC	Motion Control
Speed (°/s)	500	216
Torque (Nm)	2.2	0.7
Mass (g)	236	100
Wrist Flexor	RIC	N.A.
Speed (°/s)	450	
Torque (Nm)	2.5	
Mass (g)	153	
Elbow	RIC	LTI Boston Elbow
Speed (°/s)	80	113
Torque (N·m)	12	12.1
Passive torque (N·m)	68	68
Mass (g)	746	950

experiments show that the RIC arm satisfies the basic velocity range and linearity required for EMG control.

To assess the dynamic behavior of the actuated joints, we measured the response to different velocity step inputs for each actuated joint, except the thumb. Four different velocity step inputs were imposed and joint velocity was recorded. Each step input was repeated three times. Results of the experiments for the elbow flexor, wrist rotator, wrist flexor, and fingers flexor are shown in panels (a)–(d), respectively, of Fig. 11; different colors indicate different speed inputs. For each step input, we measured the 10%–90% rise time and overshoot, which are reported in Table II. The average rise time was 71.2, 78, 61, and 61.5 ms, for the elbow flexor, wrist rotator, wrist flexor, and fingers flexor, respectively. As can be seen from Fig. 11 and Table II, the dynamic response of the actuated joints is affected by the absolute value of the desired velocity input because of the current saturation imposed by the motor drivers. Overall the dynamic response was satisfactory, although differences between active DOFs were observed due to their different actuator and transmission configurations. As expected, the joints with higher transmission ratios showed slower velocity step responses.

Finally, modulation of RIC hand-pinch force through low-level velocity control, e.g., when interacting with a position-level constraint, such as a stiff object, was measured using an external precision load cell (Futek Advanced Sensor Technology, Inc., CA, USA), which interacted with the finger tips through a custom mechanical interface. A constant velocity set point was commanded to the finger flexors from an external PC using the CAN-bus interface, bypassing the high-level EMG-based controller. Specifically, we tested four increasing levels of velocity set points equally spaced within the finger MCP joint velocity range. For each velocity set point, we performed five repetitions, starting with the hand fully open and stopping the motor 1 s after the onset of the force interaction. Force signals from the external load cell were processed offline to obtain the average force profile and standard deviation for each velocity set point, as shown in Fig. 11(e). The maximum pinch force increased with the velocity command, reaching a peak of 84 N for the highest velocity input. Moreover, increased velocity commands generated faster force responses, showing the ability of the low-level velocity controller to modulate the dynamics of the interaction with a rigid abject. Specifically, the rising time of the force response was 0.445, 0.142, 0.113, and 0.067 ms for the 25%, 50%, 75%, and 100% velocity set points, respectively. Importantly, after a stable grasp is obtained, users can relax their muscles and let the nonbackdrivable transmission maintains a stable grip on the object.

The ability to regulate the dynamic response during physical interaction is limited in powered prostheses by the lack of force feedback [12]–[44]. In theory, a velocity controller such as the one used in the RIC arm can allow users to modulate the dynamic interaction with the environment by adjusting muscle activation level and time. In practice, this is quite difficult, as

Fig. 12. Transhumeral subject performs the Clothespin test using the RIC arm.

an equal EMG command signal result in substantially different grip force profiles when interacting with objects with different compliance—although the steady-state force will be the same. Several potential solutions have been explored to restore natural feedback, such as peripheral neural interfaces for nerve stimulation [45], [46], noninvasive haptic feedback in combination with low-level force or tactile feedback as in [12] and [13], or hybrid control approaches [47].

An endurance test was performed to determine how long the RIC arm could operate on a single battery charge. Individuals with transhumeral amputations typically wear a prosthesis for about 6 h a day [48] and perform movements for about 20% of that time (i.e., about 75 min). An external PC was programmed to send commands to the RIC arm through the CAN-bus interface, bypassing the CCU. The external program activated all active DOFs sequentially to perform the full range of motion at about half their maximum speed. Under these continuous-operation conditions, the arm moved for about 5 h and 23 min (i.e., 19360 s), and stopped when the battery voltage dropped to 10.6 V from the initial 16.1 V. As normal prosthesis use does not involve continuous movement, and no energy is required to maintain a static pose thanks to the nonbackdrivable transmission, the RIC arm can support at least a day of use on a single battery charge.

VI. Preliminary Clinical Validation

The RIC arm was tested by a subject (see Fig. 12) for 30 days at home using the pattern recognition control. The participant gave informed written consent for this research study, which was approved by the Institutional Review Board at Northwestern University. This home trial was part of a larger study, in which the subject also used a commercially available prosthetic arm comprising a Boston Elbow, a Motion Control powered wrist rotator, and an Otto Bock Sensor-hand speed.

Average prosthesis use was recorded through data logging in the prosthesis CCU. Outcome scores [49] were recorded for both prosthesis systems before the subject took the prostheses home. Specifically, we performed the Jebsen–Taylor Hand Function test [50], the 2-min box and block test, and the Clothespin test. The Jebsen–Taylor test comprises a series of activities of daily living, which includes writing a 24-letter sentence, card turning, picking up small common objects (e.g., pennies, paper clips, bottle caps), and placing them in a container, stacking checkers, simulated feeding, moving light objects (e.g., empty cans), and moving heavy objects (e.g., 1-lb weighted cans). The Clothespin test requires hand open and wrist rotation to move clothespins of different strengths from one plane to another. Both the Clothespin test and Jebsen–Taylor test are timed and lower times indicate better function. The 2-min box and block test is scored based on how many blocks are moved in 2 min; a higher score indicates better performance.

TABLE IV
Outcome Measures

	Conventional arm*	RIC arm
2-min box and Block (blocks)	7.6	11√
Clothespin (s)	119√	254
Jebsen (s)	638	566√

*Boston Elbow, motion control powered wrist rotator, Otto Bock sensor-hand speed. √ indicates better performance.

As shown in Table IV, the subject performed better on the 2-min box and block test and the Jebsen–Taylor test with the RIC arm than with the commercial arm. The subject performed worse on the Clothespin test using the RIC arm than using the commercial arm. Since the commercial arm only provided the two DOFs necessary for the Clothespin test, and so was simple to control, it was not surprising that the subject performed better using this device. Conversely, it was also not surprising that the subject performed better using the RIC arm on activities of daily living contained in the Jebsen–Taylor test, which require more DOFs such as multiple grasp patterns and powered wrist flexion.

The RIC arm worked very well during the take-home field trial, with only three failures of rapid-prototyped parts such as cosmetic coverings that were easily replaced. These parts will be injection molded in a final device for increased durability. The subject typically wore the RIC arm daily for 5–6 h durations. He appreciated the low weight and small size of the device, and was proud to demonstrate it at social functions. The subject did not report any difficulty controlling the two additional DOFs (i.e., thumb and wrist flexion). Although studies involving a larger number of subjects are needed to fully validate this finding, this initial study suggests that the RIC arm successfully meets clinical use requirements.

VII. Conclusion

The RIC arm is a 5-DOF transhumeral prosthesis that weighs only 1518 g and has the same size profile as the arm of a 25th percentile female (see Fig. 1). Compared with commercially available arms, the RIC arm provides an added wrist flexion DOF within the same mass envelope. The novel actuator design allows higher joint speeds and torques to be achieved (see Table III). In addition, the RIC arm is modular, allowing the hand to be used on persons with a transradial amputation, or allowing a different hand to be connected to the RIC arm through the universal quick-disconnect [36]. Future work will focus on evaluating the RIC arm in individuals with transhumeral amputations during home trials.

ACKNOWLEDGMENT

The authors would like to thank S. Clark, T. Kuiken, R. Lipschutz, L. Miller, T. Idstein, J. Ochoa, T. Sharkey, L. Sutton, A. Swartz, and K. Turner, for their contributions and NUPRL for preliminary motion capture.

REFERENCES

[1] R. F. ff. Weir and J. W. Sensinger, "Design of artificial arms and hands for prosthetic applications," in *Biomedical Engineering and Design Handbook*, vol. 2, M. Kutz, Ed., 2nd ed. New York, NY, USA: McGraw-Hill, 2009, pp. 537–598.

[2] D. Childress and R. F. ff. Weir, "Control of limb prostheses," in *Atlas of Amputations and Limb Deficiencies*, D. G. Smith, J. W. Michael, and J. H. Bowker, Eds., 3rd ed. Rosemont, IL, USA: American Academy of Orthopaedic Surgeons, 2004.

[3] A. Fougner, O. Stavdahl, P. J. Kyberd, Y. G. Losier, and P. A. Parker, "Control of upper limb prostheses: Terminology and proportional myoelectric control—A review," *IEEE Trans. Neural Syst. Rehabil. Eng.*, vol. 20, no. 5, pp. 663–677, Sep. 2012.

[4] E. Scheme and K. Englehart, "Electromyogram pattern recognition for control of powered upper-limb prostheses: State of the art and challenges for clinical use," *J. Rehabil. Res. Dev.*, vol. 48, no. 6, pp. 643–659, 2011.

[5] C. Cipriani *et al.*, "On the shared control of an EMG-controlled prosthetic hand: Analysis of user–prosthesis interaction," *IEEE Trans. Robot.*, vol. 24, no. 1, pp. 170–184, Feb. 2008.

[6] T. A. Kuiken *et al.*, "Targeted muscle reinnervation for real-time myoelectric control of multifunction artificial arms.," *JAMA*, vol. 301, no. 6, pp. 619–628, 2009.

[7] E. A. Biddiss and T. T. Chau, "Upper limb prosthesis use and abandonment: A survey of the last 25 years," *Prosthetics Orthotics Int.*, vol. 31, no. 3, pp. 236–257, 2007.

[8] M. S. Pinzur, J. Angelats, T. R. Light, R. Izuierdo, and T. Pluth, "Functional outcome following traumatic upper limb amputation and prosthetic limb fitting," *J. Hand Surgery, Amer. Vol.*, vol. 19, pp. 836–839, 1994.

[9] S. R. Whiteside *et al.*, *Practice Analysis Task Force*. Alexandria, VA, USA: American Board for Certification in Orthotics and Prosthetics, Inc., 2000.

[10] L. Resnik, S. L. Klinger, and K. Etter, "The DEKA arm: Its features, functionality, and evolution during the veterans affairs study to optimize the DEKA arm," *Prosthetics Orthotics Int.*, vol. 38, pp. 492–504, 2014.

[11] J. T. Belter, J. L. Segil, A. M. Dollar, and R. F. Weir, "Mechanical design and performance specifications of anthropomorphic prosthetic hands: A review.," *J. Rehabil. Res. Dev.*, vol. 50, no. 5, pp. 599–618, Jan. 2013.

[12] N. Wettels, A. R. Parnandi, G. E. Loeb, and G. S. Sukhatme, "Grip control using biomimetic tactile sensing systems," *IEEE/ASME Trans. Mechatronics*, vol. 14, no. 6, pp. 718–723, Dec. 2009.

[13] E. D. Engeberg and S. G. Meek, "Adaptive sliding mode control for prosthetic hands to simultaneously prevent slip and minimize deformation of grasped objects," *IEEE/ASME Trans. Mechatronics*, vol. 18, no. 1, pp. 376–385, Feb. 2013.

[14] D. D. Damian, T. H. Newton, R. Pfeifer, and A. M. Okamura, "Artificial tactile sensing of position and slip speed by exploiting geometrical features," *IEEE Trans. Mechatronics*, vol. 20, no. 1, pp. 263–274, Feb. 2015.

[15] M. S. Johannes, J. D. Bigelow, J. M. Burck, S. D. Harshbarger, and M. V Kozlowski, "An overview of the developmental process for the modular prosthetic limb," *John Hopkins APL Tech. Dig.*, vol. 30, no. 3, pp. 207–216, 2011.

[16] E. Biddiss and T. Chau, "Upper-limb prosthetics: Critical factors in device abandonment.," *Amer. J. Phys. Med. Rehabil.*, vol. 86, no. 12, pp. 977–87, Dec. 2007.

[17] E. Biddiss, D. Beaton, and T. Chau, "Consumer design priorities for upper limb prosthetics," *Disabil. Rehabil. Assist. Technol.*, vol. 2, no. 6, pp. 346–357, Jan. 2007.

[18] A. R. Tilley and H. Dreyfuss, *The Measure of Man and Woman: Human Factors in Design*. Hoboken, NJ, USA: Wiley, 2001.

[19] J. W. Sensinger, "Selecting motors for robots using biomimetic trajectories: Optimum benchmarks, windings, and other considerations," in *Proc. IEEE Conf. Robot. Autom.*, Anchorage, AL, USA, 2010, pp. 4175–4181.

[20] J. W. Sensinger, S. D. Clark, and J. F. Schorsch, "Exterior vs. interior rotors in robotic brushless motors," in *Proc. IEEE Conf. Robot. Autom.*, Shanghai, China, 2011, pp. 2764–2770.

[21] J. Choi *et al.*, "Design of high power permanent magnet motor with segment rectangular copper wire and closed slot opening on electric vehicles," *IEEE Trans. Magn.*, vol. 46, no. 9, pp. 3701–3704, Jun. 2010.

[22] J. W. Sensinger, "Efficiency of high-sensitivity gear trains, such as cycloid drives," *J. Mech. Des.*, vol. 135, no. 7, p. 71006, 2013.

[23] J. W. Sensinger and J. H. Lipsey, "Cycloid vs. harmonic drives for use in high ratio, single stage robotic transmissions," presented at the IEEE Conf. Robot. Autom., St. Paul, MN, USA, 2012.

[24] J. W. Sensinger and R. E. F. Weir, "User-modulated impedance control of a prosthetic elbow in unconstrained, perturbed motion," *IEEE Trans. Biomed. Eng.*, vol. 55, no. 3, pp. 1043–1055, Mar. 2008.

[25] T. Morita and S. Sugano, "Development of 4-D.O.F. manipulator using mechanical impedance adjuster," in *Proc. IEEE Int. Conf. Robot. Autom.*, 1996, pp. 2902–2907.

[26] A. Albu-Schaffer, O. Eiberger, M. Grebenstein, S. Haddadin, C. Ott, T. Wimböck, S. Wolf, and G. Hirzinger, "Soft robotics," *IEEE Robot. Autom. Mag.*, vol. 15, no. 3, pp. 20–30, 2008.

[27] J. W. Sensinger, "Unified approach to cycloid drive profile, stress, and efficiency optimization," *ASME J. Mech. Des.*, vol. 132, no. 2, pp. 1–5, 2010.

[28] C.-F. Hsieh, "Dynamics analysis of cycloidal speed reducers with pinwheel and nonpinwheel designs," *ASME J. Mech. Des.*, vol. 136, no. 9, p. 091008, Jun. 2014.

[29] M. Controzzi, C. Cipriani, and M. C. Carrozza, "Miniaturized non-back-drivable mechanism for robotic applications," *Mech. Mach. Theory*, vol. 45, no. 10, pp. 1395–1406, Oct. 2010.

[30] F. Montagnani, M. Controzzi, and C. Cipriani, "Is it finger or wrist dexterity that is missing in current hand prostheses?" *IEEE Trans. Neural Syst. Rehabil. Eng.*, vol. 23, no. 4, pp. 600–609, Jul. 2015.

[31] C. Light, P. H. Chappell, and P. J. Kyberd, "Establishing a standardized clinical assessment tool of pathologic and prosthetic hand function: Normative data, reliability, and validity," *Arch. Phys. Med. Rehabil.*, vol. 83, pp. 776–783, 2002.

[32] M. L. Zampagni, D. Casino, S. Martelli, A. Visani, and M. Marcacci, "A protocol for clinical evaluation of the carrying angle of the elbow by anatomic landmarks," *J. Shoulder Elbow Surg.*, vol. 17, no. 1, pp. 106–112, 2008.

[33] J. B. Tang, "General concepts of wrist biomechanics and a view from other species," *J. Hand Surg., Eur. Vol.*, vol. 33, no. 4, pp. 519–25, Aug. 2008.

[34] Y. Hojjat and M. Mahdi Agheli, "A comprehensive study on capabilities and limitations of roller-screw with emphasis on slip tendency," *Mech. Mach. Theory*, vol. 44, no. 10, pp. 1887–1899, 2009.

[35] A. H. R. Bellman, T. Sugar, R. D. Bellman, M. A. Holgate, and T. G. Sugar, "SPARKy 3: Design of an active robotic ankle prosthesis with two actuated degrees of freedom using regenerative kinetics," in *Proc. IEEE/RAS-EMBS Int. Conf. Biomed. Robot. Biomechatron.*, 2008, pp. 511–516.

[36] L. G. Sutton, A. Clawson, T. W. Williams, J. H. Lipsey, and J. W. Sensinger, "Towards a universal coupler design for modern powered prostheses," presented at the Myoelect. Controls Symp., Fredericton, NB, Canada, 2011.

[37] C. W. Heckathorne, "Components for electric-powered systems," in *Atlas of Amputations and Limb Deficiencies*, 3rd ed. Rosemont, IL, USA: American Academy of Orthopaedic Surgeons, 2004, pp. 145–172.

[38] A. W. Wilson, Y. G. Losier, P. A. Parker, and D. F. Lovely, "A bus-based smart myoelectric electrode/amplifier-system requirements," *IEEE Trans. Instrum. Meas.*, vol. 60, no. 10, pp. 3290—3299, Oct. 2011.

[39] E. Scheme, B. Lock, L. Hargrove, W. Hill, U. Kuruganti, and K. Englehart, "Motion normalized proportional control for improved pattern recognition-based myoelectric control," *IEEE Trans. Neural Syst. Rehabil. Eng.*, vol. 22, no. 1, pp. 149–157, Jan. 2014.

[40] C. Toledo, A. Simon, R. Muñoz, A. Vera, L. Leija, and L. Hargrove, "A comparison of direct and pattern recognition control for a two degree-of-freedom above elbow virtual prosthesis," in *Proc. IEEE Annu. Int. Conf. Eng. Med. Biol. Soc.*, 2012, pp. 4332–4335.

[41] C. L. Chicoine, A. M. Simon, and L. J. Hargrove, "Prosthesis-guided training of pattern recognition-controlled myoelectric prosthesis," in *Proc. IEEE Annu. Int. Conf. Eng. Med. Biol. Soc.*, 2012, vol. 60611, pp. 1876–1879.

[42] V. J. Majd and M. a. Simaan, "A continuous friction model for servo systems with stiction," in *Proc. Int. Conf. Control Appl.*, 1995, pp. 296–301.

[43] M. R. Kermani, R. V. Patel, and M. Moallem, "Friction identification and compensation in robotic manipulators," *IEEE Trans. Instrum. Meas.*, vol. 56, no. 6, pp. 2346–2353, Dec. 2007.

[44] A. Ninu, S. Dosen, S. Muceli, F. Rattay, H. Dietl, and D. Farina, "Closed-loop control of grasping with a myoelectric hand prosthesis: Which are the relevant feedback variables for force control?" *IEEE Trans. Neural Syst. Rehabil. Eng.*, vol. 22, no. 5, pp. 1041–1052, Sep. 2014.
[45] S. Raspopovic *et al.*, "Restoring natural sensory feedback in real-time bidirectional hand prostheses," *Sci. Transl. Med.*, vol. 6, no. 222, 2014.
[46] D. W. Tan, M. A. Schiefer, M. W. Keith, J. R. Anderson, J. Tyler, and D. J. Tyler, "A neural interface provides long-term stable natural touch perception," *Sci. Transl. Med.*, vol. 6, no. 257, 2014.
[47] B. A. Kent, N. Karnati, and E. D. Engeberg, "Electromyogram synergy control of a dexterous artificial hand to unscrew and screw objects," *J. Neuroeng. Rehabil.*, vol. 11, no. 1, 2014.
[48] W. J. Gaine, C. Smart, and M. Bransby-Zachary, "Upper limb traumatic amputees. Review of prosthetic use," *J. Hand Surg. Amer.*, vol. 22 B, no. 1, pp. 73–76, 1997.
[49] L. A. Miller and S. Swanson, "Summary and recommendations of the Academy's State of the Science conference on upper limb prosthetic outcome measures," *J. Prosthetics Orthotics*, vol. 21, pp. 83–89, 2009.
[50] R. H. Jebsen, N. Taylor, R. B. Trieschmann, M. J. Trotter, and L. A. Howard, "An objective and standardized test of hand function," *Arch. Phys. Med. Rehabil.*, vol. 50, no. 6, pp. 311–319, 1969.

Tommaso Lenzi (S'11–M'13) received the M.Sc. degree in biomedical engineering from the University of Pisa, Pisa, Italy, in 2008, and the Ph.D. degree in biorobotics from Scuola Superiore Sant'Anna, Pisa, in 2012.

He is currently a Research Scientist with the Center for Bionic Medicine, Rehabilitation Institute of Chicago, Chicago, IL, USA, and with the Department of Physical Medicine and Rehabilitation, Northwestern University, Chicago. He has co-authored 19 ISI journal papers and 31 peer-review conference proceedings papers. His main research interests include robotics, mechatronics, and rehabilitation medicine, with a major emphasis on the design and control of wearable robots for human assistance and rehabilitation.

James Lipsey received the B.E. and M.Sc. degrees in mechancal engineering from Vanderbilt University, Nashville, TN, USA, in 1994 and 1997, respectively.

He is currently the Mechanical Engineering Manager with the Center for Bionic Medicine, Rehabilitation Institute of Chicago, Chicago, IL, USA.

Mr. Lipsey is a licensed Professional Engineer in the state of Illinois.

Jonathon W. Sensinger (M'09–SM'16) received the B.S. degree in bioengineering from the University of Illinois, Chicago, IL, USA, in 2002, and the Ph.D. degree in biomedical engineering from Northwestern University, Chicago, in 2007.

He is the Associate Director with the Institute of Biomedical Engineering and an Associate Professor of Electrical and Computer Engineering with the University of New Brunswick, Fredericton, NB, Canada. His research interests include body-powered and robotic prosthesis, and exoskeleton design and control. In addition, he performs research on human–machine interfaces using haptics and computational motor control approaches with a goal to improve the control filtering and sensory feedback options available to persons with an amputation.

Dr. Sensinger is a member of the Association of Professional Engineers and Geoscientists of New Brunswick.